Applied Thermal Engineering 197 (2021) 117408

Contents lists available at ScienceDirect

Applied Thermal Engineering

journal homepage: www.elsevier.com/locate/apthermeng

Simultaneous and consecutive charging and discharging of a PCM-based domestic air heater with metal foam

Jasim M. Mahdi [a], Hayder I. Mohammed [b], Pouyan Talebizadehsardari [c,*], Mohammad Ghalambaz [d,e], Hasan Sh. Majdi [f], Afrasyab khan [g], Wahiba Yaïci [h], Donald Giddings [c]

[a] Department of Energy Engineering, University of Baghdad, Baghdad 10071, Iraq
[b] Department of Physics, College of Education, University of Garmian, Kurdistan, Iraq
[c] Faculty of Engineering, University of Nottingham, University Park, Nottingham NG7 2RD, UK
[d] Metamaterials for Mechanical, Biomechanical and Multiphysical Applications Research Group, Ton Duc Thang University, Ho Chi Minh City, Vietnam
[e] Faculty of Applied Sciences, Ton Duc Thang University, Ho Chi Minh City, Vietnam
[f] Department of Chemical Engineering and Petroleum Industries, Al-Mustaqbal University College, Babylon 51001, Iraq
[g] Institute of Engineering and Technology, Department of Hydraulics and Hydraulic and Pneumatic Systems, South Ural State University, Lenin prospect 76, Chelyabinsk 454080, Russian Federation
[h] CanmetENERGY Research Centre, Natural Resources Canada, 1 Haanel Drive, Ottawa, Ontario, Canada

ARTICLE INFO

Keywords:
Latent heat storage
Domestic space heating
Phase change materials
Simultaneous and consecutive phase change
Mode of operation
Storage-air heater

ABSTRACT

Numerical investigations of the melting/solidification in a metal foam saturated with phase change material (PCM) were performed for simultaneous and consecutive operational modes. The composite is embedded in a rectangular compound cooled by passing air in a middle channel which is then employed to heat the room as a space heater. The composite is heated by two-rod heating elements to store thermal energy for peak-shaving purposes. The study covered the evaluation of the system in different operational modes for charging and discharging rate, the impacts of the metal foam and the influence of coolant flow rate on the solidification performance. The presence of PCM on one hand due to having almost constant temperature during the phase change process and the use of metal foam on the other hand due to proving high heat transfer rate from the PCM to the coolant, help in providing a uniform output temperature from the system which is a key factor for highly efficient space heaters. Moreover, evaluation of the operational modes can help to understand the behavior of the system in real scenarios when there is a need to charge the storage system and heat the room (discharging) simultaneously. The results show that the melting process is fully achieved due to the faster-charging process rate in modes I (8-hour charging and 8-hour discharging separately) and III (2-hour charging and 14-hour simultaneous charging-discharging), compared with mode II (2-hour charging and 2-hour discharging separately, repeated for 16 h). The temperature distribution in Mode III was more constant, which produced uniform heat exchanged between the PCM and the cooling fluid. The porosity is inversely proportional to the liquid development rate. The PCM melts entirely within 6.5 h for 90% porosity while 78% of the PCM melts in 8 h for the 95% porosity case. The final mean PCM temperature changed from 69.9 °C to 66.4 °C, when the air flow rate increases from 0.01 kg/s to 0.03 kg/s.

1. Introduction

Interest in thermos-physical applications based on thermal energy storage (TES) is increasing since it contributes to the reduction of pollution and undesirable greenhouse gas emission [1]. TES systems are frequently used due to intermittency of the source of, and the demand for, energy [2]. The challenge is to store and release the energy so that it can be converted efficiently into required forms [3]. Phase change material (PCM) offers high energy storage capacity and constant phase change temperature suitable for heating/cooling applications. Latent heat released by PCM (based on the heat release when the phase change process of the PCM occurs) presents greater volumetric storage capacity (5–14 times) than the sensible heat units [4]. In 1975, the first latent

* Corresponding author.
E-mail addresses: pouyan.talebizadehsardari@brunel.ac.uk, ptsardari@gmail.com (P. Talebizadehsardari), mohammad.ghalambaz@tdtu.edu.vn (M. Ghalambaz).

https://doi.org/10.1016/j.applthermaleng.2021.117408
Received 23 November 2020; Received in revised form 27 July 2021; Accepted 29 July 2021
Available online 2 August 2021

Nomenclature

A_m	The mushy zone constant (kg/m^{3}s)
C	Inertial coefficient
C_p	PCM specific heat (J/kgK)
C_s	Solid specific heat (J/kgK)
g_i	Gravitational acceleration (m/s^2)
k_e	Effective thermal conductivity (W/mK)
k_f	PCM thermal conductivity (W/mK)
k_s	Solid thermal conductivity (W/mK)
K	Permeability (m^2)
L	Latent heat of fusion (J/kg)
m	PCM mass (kg)
P	Pressure (Pa)
Q	Heat storage/retrieval capacity (J)
$\dot{Q}$	Heat storage/retrieval rate (J)
t_m	Melting/solidification time (s)
T	Temperature (K)
T_i	Initial PCM temperature (K)
$T_{liquidus}$	Liquidus temperature (K)
T_e	End temperature of simulation (K)
T_m	Melting point temperature (K)
T_{ref}	Reference temperature (K)
$T_{solidus}$	Solidus temperature (K)
u_i	Velocity component (m/s)
$\vec{V}$	Velocity vector (m/s)

Greek symbols

β	Thermal expansion coefficient (1/K)
ε	Porosity
λ	Liquid fraction
μ	Dynamic viscosity (kg/ms)
ρ	Density (kg/m^3)
ρ_m	Density at melting point (kg/m^3)
ρ_s	Density of solid (kg/m^3)
ΔH	Latent heat (J/kg)

Subscripts

ref	Reference

heat storage (LHS) application was investigated by Telkes [5]. PCMs have applications in different areas represented in a large number of papers as collected in reviews of the area, such as energy-reduction buildings [6]. solar still [7]. solar cooker [8]. waste heat recovery [9]. solar power plants [10]. solar air heater [11]. Trombe walls [12]. cold storages [13]. thermal comfort in vehicles [14] and electronic cooling [15,16].

The issue with the PCM is the weak thermal conductivity and consequently low heat transfer [17,18]. The most frequent techniques for improving the heat transfer include adding extended parts such as fins and heat pipes or applying multiple-segment conductive foam / PCMs (with various melting and solidification points) composites [19–21]. Bayón et al. [22] used graphite fins to improve the heat transfer in the prototype LHES system with a KNO_3/$NaNO_3$ type of PCM. They assumed a quasi-static mathematical technique to assess the thermal efficiency of the graphite/PCM combination. Yang et al. [23] stated that the performance of the energy system enhances by using fins and the smallest fins cause a slower melting rate due to smaller heat transfer surface area. Rathod et al. [24] experimentally studied the effect of fins on the efficiency of melting and solidification processes rates in a shell-and-tube LHTES system. The findings suggest that with an inlet temperature of 80 °C and 85 °C with the presence of fins, the melting rate reduced by 12.5% and 24.52%, respectively, compared with the system without fins. Sciacovelli and Verda [25] numerically studied the effect of Y-shaped fins planted in a shell-and-tube LHTES system. They found the efficiency of the unit enhances by 24%. They observe that a wide angle between the branches of the fins enhances the phase change rate and vice versa. Al-Abidi et al. [26] numerically studied the PCM charging period in a triplex finned-tube heat exchanger. They found that the thickness of the fins has insignificant influences on the phase change rate unlike the size and the quantity of the fins, which have a great impact on the process. Hosseinizadeh et al. [27] examined the influence of the internal fins in a rectangular heat sink system. They found that the quantity and the size of the fins considerably improved the efficiency of the unit while change due to thickness was negligible. Li et al. [28] numerically studied the efficiency of the TES system with a multi-PCM with different volume ratio having different phase change temperatures and water was used as the cooling fluid. They show that a TES system using volumetric ratio of 1:2:3 accelerates the melting rate in comparison with applying an alone PCM and the full charging capacity of the multi-PCM TES system with a 1:2:3 vol ratio was 3.637 MJ and raised by 32% as compared to the alone PCM. Sefidan et al. [29] numerically evaluated the discharging process, phase change rate and temperature distribution of multiple PCM volumes in a finned triplex tube. Difference of liquid fraction values, minimum temperatures multi-PCM are stated for improved insight into the heat transfer features of the LHTES unit to allow uniform solidification designs and balance the solidification rate within the whole annulus.

Combining a nanomaterial with PCMs [30–34], nanoencapsulation of PCMs [35–38], use of high conductivity metal foams [39–42] and modifying the geometry of the heat exchanger have also received attention. Research, based on numerical simulation of the latent-heat energy storage processes, has earned considerable interest as a means of optimising storage and release [43]. Zivkovic and Fuji [44] theoretically studied the charging rate of PCMs in horizontal axis rectangular and cylindrical containers. They found that the PCM in the rectangular shape melts faster than the cylindrical shape for the same volume and heated surface area. A numerical study of evaluating the PCM melting rate of three various enclosures (rectangular, cylindrical and shell and tube was performed by Vyshak and Jilani [45]. They found that the shell-and-tube geometry is fastest at responding to the melting processes for the same energy supplied. A review of the latent heat thermal energy storage systems (LHTESS) regarding the shape of the PCM containers by Agyenim et al. [46]. They notice that the shell-and-tube energy storage system is the most widely studied among those systems. The solidification rate of the PCM in the shell and tube storage system is much faster than the rectangular configuration storage as stated by the numerical analyses by Mosaffa et al. [47,48]. Ho and Gao [49] experimentally investigated the influence of nanoparticles on heat transfer during the charging mechanism in a vertical container filled with alumina/n-octadecane nano-PCM. They found that nanoparticle concentration (determined locally by the intensity of melting) is inversely proportional to the natural convection in the melting area [50]. Kumaresan et al. [51] investigate the impacts of multi-wall carbon nanotube (MWCNT) in liquid paraffin (as the PCM) on thermal performance. The thermal conductivity of the composite is proportional to the MWCNT concentration. Ghalambaz et al. [52] addressed the free convection process of nanofluids/hybrid in a container. The results show that using hybrid

nanofluids enhances the free convection heat exchange. However, using such hybrid-nanofluids in porous spaces (metal foams) could reduce the heat transfer by suppressing the natural convection flows [53]. Ebadi et al. [54] studied the influence of nanoparticles on a bio-based nano PCM in a cylindrical TES unit. They found that the early stage of the charging process showed the same behaviour with or without nanoparticles, but during the phase change process, the nanoparticles made the process faster than the pure PCM [55]. Pal Singh et al. [56] examined the improvement in the viscosity of nano-PCM in a solar cooling TES unit using a novel fin design. They found that the maximum drop of 43% in the charging rate is detected for TES with the fin (at 5 vol% nanoparticles) and the reducing fin size provided the highest rate of heat transfer. Mahdi and Nsofor [57] numerically examined the influences of combining Al_2O_3 nanoparticles on the solidification (discharge) of a PCM in a triplex-tube TES. They found that adding 3 and 8 vol% of nanoparticles saves 8% and 20% of the total time, respectively. However, the nanoparticles did not display any effect at the initial stage of the discharge process. In a separate study, Mahdi and Nsofor [58] investigated the heat-transfer improvement in PCM in a shell-and-tube TES system by arranging multiple segments of conductive foam in the PCM to reflect the decay of intensity of heat transfer away from the heat source. They found an enhancement in the energy storage and reduction in the phase changing time by using multiple segments. Sardari et al. [59] investigated numerically the influence of different variables on the PCM charging process in a vertical heat storage system filled with a Cu metal multi-segment foam. The Cu foam gives high performance for the charging process by reducing the charging rate to 85% of the time of the PCM only situation. They also showed that the multiple-segment porous unit decreased the charging rate by 3.5% compared with the case of uniform porosity.

Because of the high thermal efficiency of LHS systems, they are widely used in building applications [60–62]. Zhou et al. [63] reviewed the applications of combining the PCM with the building materials to avoid energy losses. Souayfane et al. [64] investigated the impact of the PCM on the building cooling process. The PCM, which recharge after usage was added as the energy storage material in the building shield. Zalba et al. [65] experimentally, studied the storing of the absorbed energy in the daytime for the cooling process. The challenges of applying PCM in buildings could be represented as the limited area, structure, design, position, and climate [66]. Experimentally, different patterns of PCM blocks applied as a TES in a cooling unit for ideal building was analyzed by Yamaha et al. [67]. They stated that the room temperature could be settled in the comfortable range for 3 h when a 5.4 kg PCM per square meter was used. Waqas and Kumer [68] combined a PCM with a solar system to warm a specific room. The system was affected by the heat transfer fluid flow, PCM volume, and optimized to achieve the best performance possible. Sardari et al [69] presented the application of composite porous/PCM in energy storage air heaters in domestic buildings showing the advantages of the metal for providing uniform output air temperature. They employed a rectangular heating element on the walls of the PCM shell to charge the system.

Although extensive research has been carried out on numerous types of thermal storage systems for different applications, the idea of investigating different modes of operation regarding the simultaneous and consecutive charging/discharging of latent TES applicable to domestic air heaters has not yet been investigated. The simultaneous charging/discharging can solve the problem of the large volume of the storage heaters by reducing the amount of required PCM which can also be more cost-effective. However, the output temperature of the heater as a key parameter as well as the energy level of the TES should be investigated for different modes of simultaneous charging/discharging to understand the performance of the system properly. Thus, the effort in this work was devoted to analysing how the outcome of an air heater in various operational modes can be enhanced with the inclusion of conductive foam-PCM composite to improve the thermal conductivity and thermal diffusion inside the bulk PCM as well as heat transfer rate from the PCM to the cooling fluid. To examine the effective role of applying porous foam in the context of PCM melting/solidifying enhancement potential, a 3D computational fluid dynamic model (CFD) based on a finite-volume discretization approach was developed and validated. Transient behaviour of the molten PCM due to the interstitial heat transfer generated by the foam skeleton and temperature-dependent thermophysical properties of PCM were considered in the model developed. Temporal behaviour of the PCM-foam composite under three different modes of operation were considered to reliably check the effect of operating mode on the phase-transition rate and temperature distribution as well as output temperature of the heater. The results from this study are expected to contribute to more efficient and compact thermal storage systems for domestic air-heating applications. The advantage of this study is to evaluate the optimum operating state considering the properties of the metal foam, and the flow condition of the heat transfer fluid as well as investigating the bast pattern of the charging and the discharging process which can help minimize the size of the heat exchanger by introducing simultaneous charging/discharging mechanism.

2. System description

The schematic of the proposed storage unit is illustrated in Fig. 1-a. Since the proposed system is used as a storage heater for domestic space heating, a rectangular shape is selected which is similar to the normal radiators. Metal foam-PCM is placed in equal rectangular containers at the side of an air channel wall but other walls are adiabatic. Two heating rod elements (length of 25 cm and diameter of 1 cm) with a fixed temperature of 95 °C are placed inside the metal foam-PCM. Note that the implementation of the heating elements in the centre of the PCM solves the shrinkage problems of PCM and causes a uniform distribution of thermal energy in the domain. There is a copper shield (thickness of 1 mm) that separates the air channel from the PCM enclosure, which allows the heat to flow from the PCM to the air. The size of the PCM enclosure is 15 × 30 × 50 cm. Thus, the mass of PCM in the container is almost 15.32 kg. The width of the air channel is 2 cm. Note that as shown in Fig. 1, due to symmetrical conditions of the problem, only one-quarter of the domain is modeled numerically. Aluminum foam is employed with a fixed pore density of 30 PPI (pores per inch) and porosity of $\varepsilon =$ 0.90 and 0.95. Porosity is the ratio of the pore volume where PCM is to be embedded to the entire volume of pores and ligaments. The range of porosity in this analysis was limited to 0.90/0.95 to avoid altering much of the PCM volume usage which in turn impacts the unit capacity to the storage/retrieval of thermal energy. Meanwhile, the whole unit is set primarily at 21 °C. It is found that the charging mode (melting) is done within 8 h, then the discharging is initiated to allow the flowing of heat from the PCM to the air in the next 16 h. It should be noted that due to the governing conditions of the problem, the computational domain is considered symmetric in two planes in two vertical planes. The symmetrical boundary condition can be employed when the physical domain (geometry) and the expected flow field pattern of the developed solution are mirrored along that surface. The studied geometry is a rectangular shell which symmetrical in two vertical planes. For the fluid flow pattern, due to movement of the liquid PCM under natural convection effect, the pattern of the fluid flow is also symmetrical about the middle vertical planes which have been also reported in the literature [69,70]. Thus, it is possible to consider just a quarter size of the domain to reduce computational cost.

The working principle of the system can be described as: (1) During the charging mode (Fig. 1-b), the air passages are blocked and insulated from the top and bottom. (2) During discharging (Fig. 1-c), the air passes through the air passages by an air blower to warm up and then heat the room from the top of the system. Different air flow rates are evaluated during the discharging process for the purpose of space heating. (3) For the simultaneous charging/discharging (Fig. 1-d), both the heating elements and air blower are on to charge the PCM by the heating elements

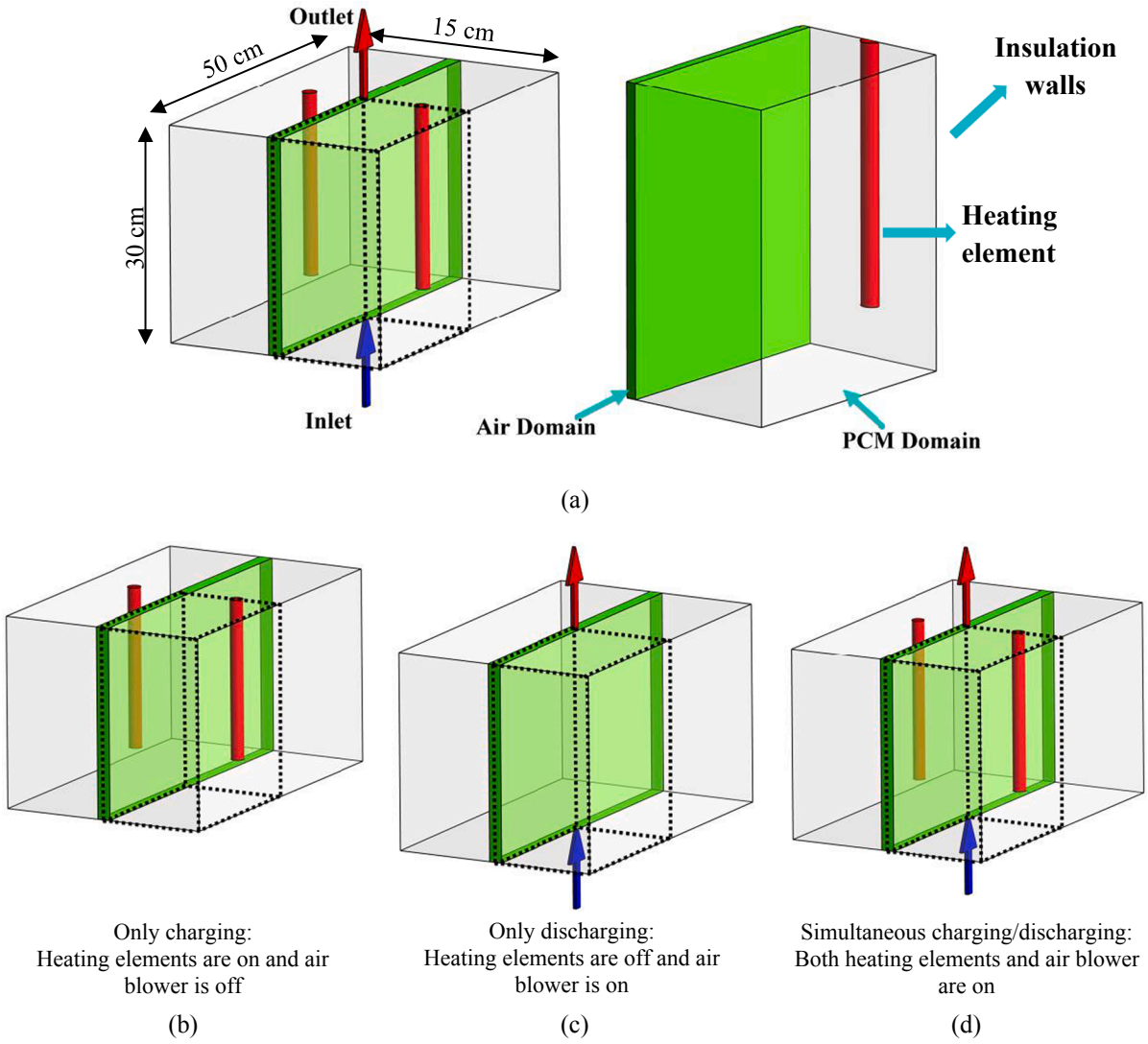

Fig. 1. The proposed metal foam-PCM with air heat exchanger: a) boundary conditions and b, c and d) working principles in charging, discharging, simultaneous charging/discharging, respectively.

and at the same time discharge the stored heat to the room through passing the air from the middle of the storage unit.

To provide various operational modes, a control system should be provided to turn on/off the supplying heating elements in the charging mode as well as the air blower in the discharging mode to release the stored heat to the building. This study focused on the LHTES to figure out the performance of the system in the mode of simultaneous charging/discharging of the unit. As mentioned, the reason is to provide a more compact unit which can save the cost, mass and volume of the storage unit ease them for more commercial usages.

The PCM material, which used in this work is proposed to be RT70HC (RUBITHERM) [71]. Its nominal properties as provided by the manufacturer are shown in Table 1. This material is an organic PCM with an unlimited lifetime and high energy storage density. It also has a melting temperature range (T > 60 °C), which applies to air heating applications [72]. Note that the inlet air temperature is 21 °C during the solidification considering different mass flow rates of 0.01, 0.02 and 0.03 kg/s. Note that the flow rate is considered 0.02 kg/s in the whole study except in the study of the flow rate.

Table 1
Properties of RT70HC [73].

Property	RT70HC
Solidus temperature	69 °C
Liquidus temperature	71 °C
Heat of fusion	260000 J/kg
Specific heat	2000 J/kg K
Density	880 kg/m^3 (solid) – 770 kg/m^3 (liquid)
Thermal conductivity	0.2 W/mK
Viscosity	0.0056 Pa.s
Expansion coefficient	0.001 1/K

3. Numerical modeling

This study continues the investigation and method described in [74] and [75]. For the phase transition, the enthalpy-porosity method is applied while the thermal-equilibrium approach is utilized for modeling the heat transfer in the porous structure [76]. The governing equations for incompressible Newtonian fluid flow of PCM in a homogeneous and isotropic porous medium are given here as previously presented in [74] with more details:

$$\frac{\partial \rho}{\partial t} + \nabla . \rho \vec{V} = 0 \quad (1)$$

$$\frac{\rho}{\varepsilon}\left[\frac{\partial \vec{V}}{\partial t}+\nabla\left(\frac{\vec{V}.\vec{V}}{\varepsilon}\right)\right]=-\nabla P+\frac{\mu}{\varepsilon}\nabla^2\vec{V}-A_m\frac{(1-\lambda)^2}{\lambda^3+0.001}\vec{V}-\left(\frac{\mu}{K}+\frac{\rho C\left|\vec{V}\right|}{\sqrt{K}}\right)\vec{V}-\rho\vec{g}\beta(T-T_{ref}) \quad (2)$$

$$(1-\varepsilon)\rho_s C_s\frac{\partial T}{\partial t}+\rho C_p(\varepsilon\frac{\partial T}{\partial t}+\vec{V}.\nabla T)=k_e\nabla^2 T \quad (3)$$

where A_m is the mushy-zone parameter which is estimated at 10^5–10^6 by most preceding researchers [77]. It is found in the present analysis that a value of $A_m = 10^5$ best matches the Zhao et al.'s experimental results [78,79] that are used in the validation of the present results. The Boussinesq approximation (last term in Eq. (2)) is added to the momentum equation for the buoyancy effect where the reference temperature is the melting point temperature, which is the median of solidus and liquidus temperatures. k_e is the thermal conductivity of the composite (porous medium and PCM) and given as:

$$k_e=(1-\varepsilon)k_s+\varepsilon k_f \quad (4)$$

λ is defined by:

$$\lambda=\frac{\Delta H}{L}=\begin{Bmatrix} 0 if T<T_{Solidus} \\ 1 if T>T_{Liquidus} \\ \frac{T-T_{Solidus}}{T_{Liquidus}-T_{Solidus}} if T_{Solidus}<T<T_{Liquidus} \end{Bmatrix} \quad (5)$$

where ΔH is the fractional PCM latent heat.

For the airflow simulation, the impacts of metal foam and phase change are eliminated from the governing equation results in the conventional forms of Navier-Stokes equations for laminar fluid flow and heat transfer in the channel [76].

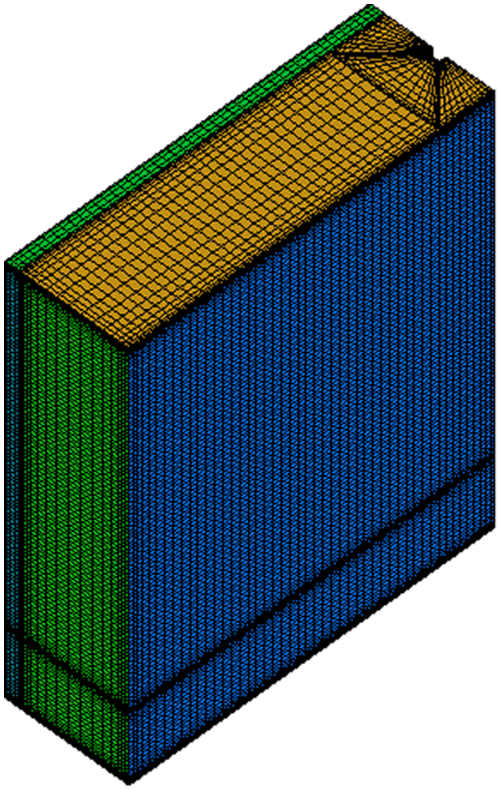

Fig. 2. The generated mesh in the symmetrical condition.

4. Numerical procedure and validation

ANSYS-FLUENT computational fluid dynamics (CFD) commercial package is employed in this study to solve the governing equations using the SIMPLE algorithm. The PRESTO and QUICK schemes, respectively, are utilized for pressure correction and momentum and energy equations. The convergence criteria are set to 10^{-4} for continuity and 10^{-6} for the momentum and energy equations. Fig. 2 shows the generated meshes using two heating elements inside the domain. The model is mirrored on two vertical planes using symmetry boundary conditions for the vertical surfaces and thus only one quarter of the whole domain is modeled numerically.

The number of cells for the computational domain is 195,000. A denser mesh with 426,700 cells is also generated to reach the independent results from the number of grids based on the melting rate and average temperature of the PCM. The results show no considerable effect and the differences between the liquid fraction and average temperature of the PCM for the cases with 195,000 and 426,747 cells are less than 0.2% after 8 h for the case with 95% porosity are and therefore the grid number of 195,000 is selected for further investigations. Note that a denser mesh was generated near the wall region which is one of the reasons for the negligible difference between the results of cases with 195,000 and 426,700 cells.

For the numerical code verification, the study of Zhao et al. [79,80] is regenerated employed also in Liu et al. [78] for simulating a rectangular LHS unit with a heated wall from the bottom using a copper porous structure inside the PCM (RT-58). Since in this study, a similar geometry is proposed using composite PCM/metal foam, the geometry used by Zhao et al was chosen to verify the code. For the current geometry, heat loss is also considered for the container walls except the bottom using constant heat flux which provides more accurate data to prove the validity of the model. The porosity and pore density of the metal foam are 95% and 10 PPI, respectively. The dimensions of the considered energy storage unit are 200 mm and 25 mm in × and y-directions, respectively. Fig. 3 shows the variation of temperature at the location of 0.8 cm from the bottom in comparison with the results of Liu et al. [53] using both thermal equilibrium and non-equilibrium models as well as experimental data of Zhao et al. [52] illustrating an acceptable agreement. It should be noted that a user-defined function (UDF) was developed to model the metal foam in non-equilibrium thermally condition

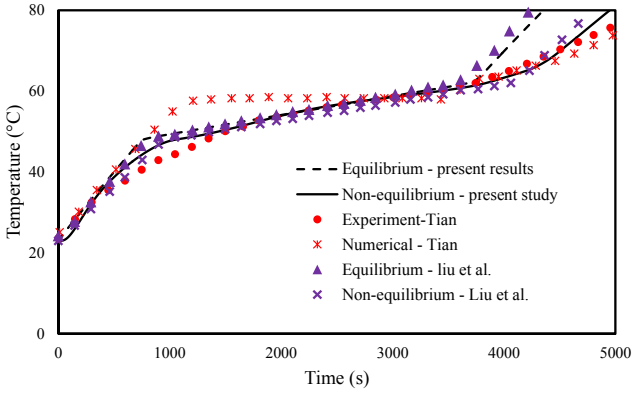

Fig. 3. Validation results in comparison with the experimental and numerical studies in the literature [78,79]

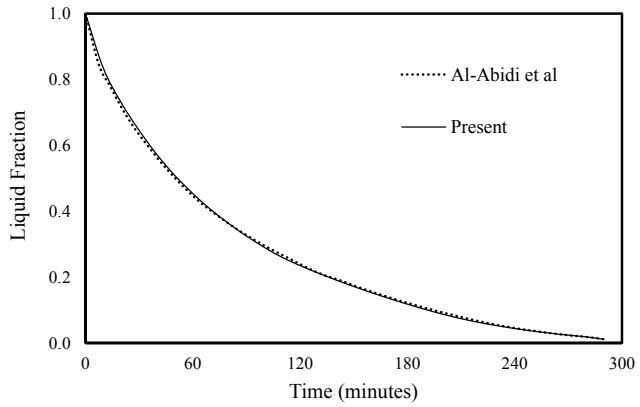

Fig. 4. Validation results in comparison with Al-Abidi et al.'s results [81]

considering variable convection heat transfer coefficient inside the liquid PCM in the pores of the foam which is defined as a function of liquid PCM velocity [75]. The developed UDF provides more accurate results as shown in Fig. 3 as well as the study of Liu et al.

To provide further trust of the present model's predictions, the present results were also validated via the results reported by Abidi et al. on the solidification of paraffin RT82 in a triplex-tube heat exchanger. The list of boundary conditions and physical properties of PCM used in the reference study is applied, and the liquid-fraction profile predicted based on the present model is compared with that from Abidi et al.[81]. A very good agreement is achieved between the two studies as shown in Fig. 4.

The non-equilibrium model can predict the PCM liquid fraction more accurately compared to the equilibrium model. However, due to the high computational cost of the thermal non-equilibrium method for modeling the liquid phase behavior in the porous medium especially in 3D simulations, the thermal equilibrium model was employed for further studies. It was shown in the authors' previous study that the difference between the thermal equilibrium and non-equilibrium models is small due to the primary domination of heat conduction rather than the natural convection effect [75]. The average velocity of PCM in the presence of metal foam is in the order of 10^{-6} showing the lower effect of natural convection while it is in the order of 10^{-4} for the PCM only case. Therefore, in this study, the equilibrium model was used.

Worth noting that the main limitation of the numerical models is the idealization presented in the system description and the exact calculation according to the equation and the assumption presented in the mathematical model, which produces a cap (even inconsiderable) between the model and the experiment. As presented in the validation with experimental data, the assumptions have a limited impact on the results of the process. Increasing the number of assumptions (to simplify the calculation processes) decreases the reliability and the accuracy of the outcome which are not significant according to the presented validation.

5. Results and discussion

The operating conditions, materials and heat-exchanger size are the essential parameters for the successful design of any typical energy storage system. In this study, the essential storage load, heat-exchanger dimensions, and air flow conditions are considered to design an effective latent-heat storage unit. The heat storage load, specific heat and latent heat of PCM are the main parameters that specify the efficacy of PCM for use as a TES medium. The porous aluminum (Al) foam is used for additional performance improvement in the TES system. The target is set for the PCM melting part of the cycle to be ended within 8 h, followed by a period of 16 h for solidification. The operating time for the charging mode (melting) is between 12 PM and 8 AM. For the discharging mode (solidification), the operating time is from 8 AM to 12 PM. The thermal comfort temperature is expected to be 21 °C in the current study.

The liquid-fraction contours and temperature distributions for the case of porosity of 90% and the air flow rate of 0.02 kg/s for melting mode are shown in Figs. 5 and 6, respectively. It should be noted that during the melting, the air passages are blocked and insulated from the top and bottom. Similar trends are observed over longer solidification periods for the non-porous case. The temperature of the domain starts to rise as heat moves to the PCM. The melting started when the PCM achieved the phase-change (critical) temperature (69 °C). The heat distribution is enhanced by the high thermal conductivity of the embedded porous medium (Al). Melting PCM (liquid phase) rises by natural convection and produces an inverted cone profile. Within 2 h, 50% of the domain is liquid, however, the rest melts more slowly because of the increasing distance from the source and the low thermal convection heat transfer. The total domain melts within 8 h as shown in

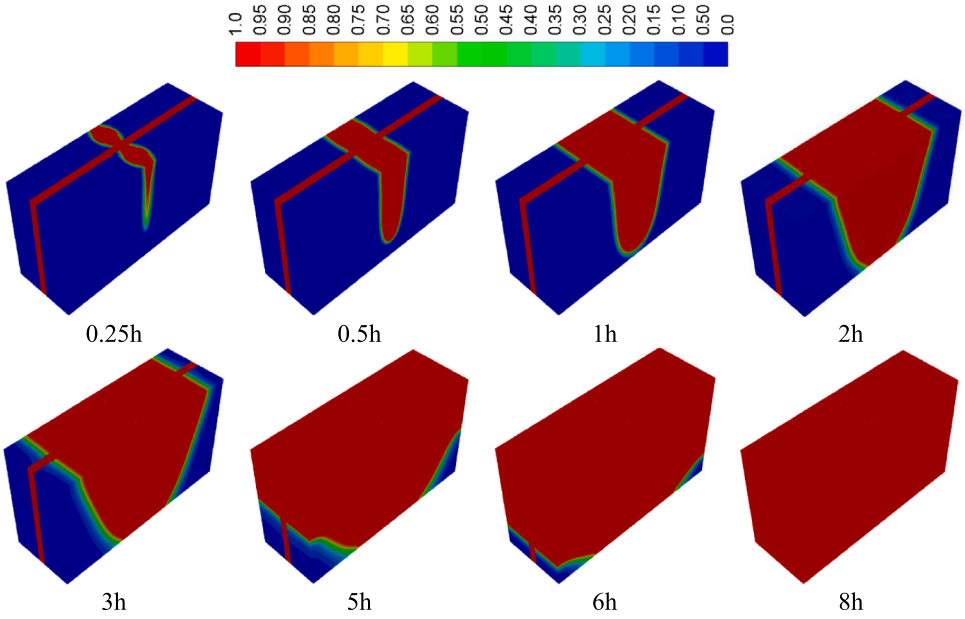

Fig. 5. Development of the liquid fraction contours during 8 h of the charging mode (melting).

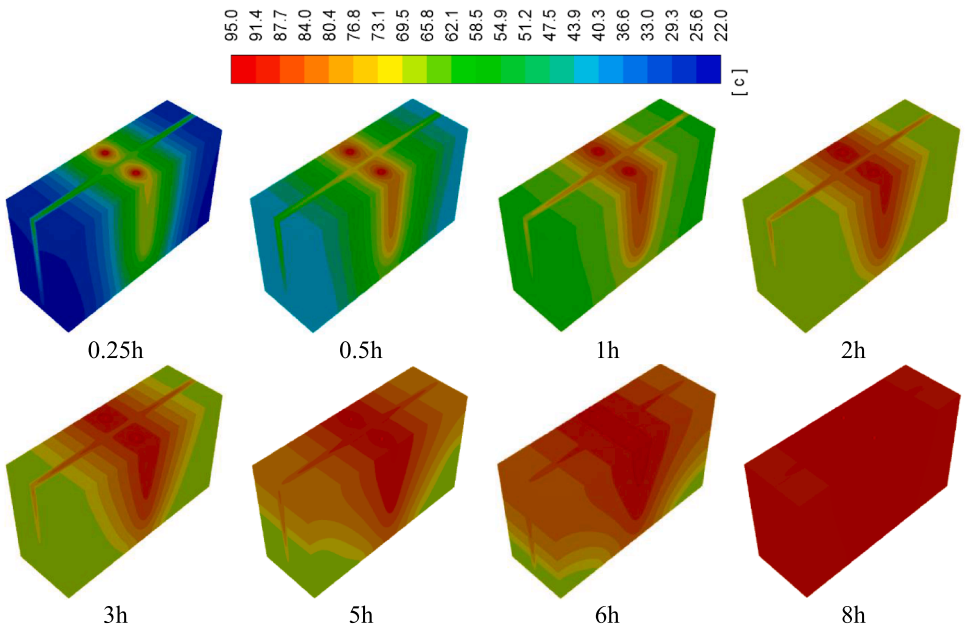

Fig. 6. Development of the Temperature contours during 8 h of the charging mode (melting).

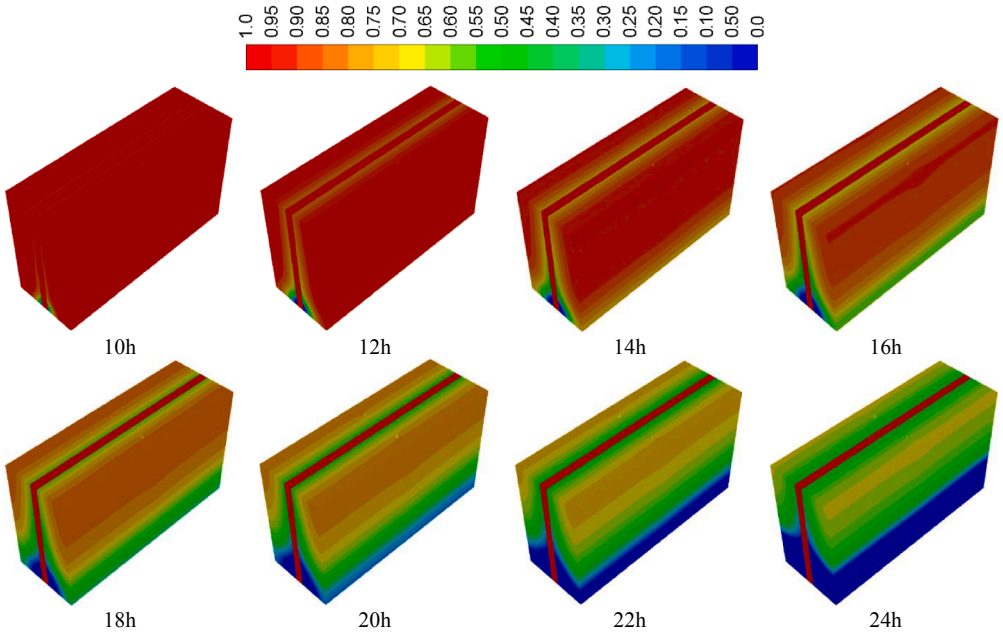

Fig. 7. Development of the liquid fraction during 16 h (8 h-24 h) of the discharging mode (solidification).

Fig. 5. The higher temperature appears on the liquid phase and takes a cone shape. After 2 h, the average temperature is 348 K with higher values around the heat source, then after 8 h, the temperature becomes 365 K as shown in the last image in Fig. 6.

When the unit becomes fully charged (after 8 h), the heat supply is cut off and the solidification (discharge) process commences. Fig. 7 illustrates that the liquid fraction shrinks; the bottom part of the unit is early solidified due to the transfer of conductive heat in the top part and discharging (releasing) heat to the airflow by free convective heat transfer, the rate of which decreases in the channel as the temperature varying between air and PCM reduces with height. After 24 h, the data show that 45% of the PCM is solid, and the rest remains liquid. This means that 55% of the heat store in the domain is unchanged.

5.1. Charging mechanism dependence on porosity of composite PCM

Fig. 8 shows the time-dependent development of the PCM liquid-fraction during melting for three different foam-PCM cases: no porous material-PCM ($\varepsilon = 1$), porous-PCM $\varepsilon = 0.90$ and porous-PCM $\varepsilon = 0.95$. By adding a porous material into the PCM, due to higher rate of heat transfer in the domain and also from the heating element to the PCM, thermal energy is stored quicker in the PCM; thus, the cases with the presence of metal foam show higher liquid fraction of the PCM in an identical time compared with the no porous case. The liquid-fraction curve for the case of lower porosity $\varepsilon = 0.90$ rises much faster up than the other cases of non-porous and $\varepsilon = 0.95$. The liquid fraction in the 0.9 case reaches its maximum value of 1 indicating completely melted within 7 h. However, in other cases, longer operating time is needed to

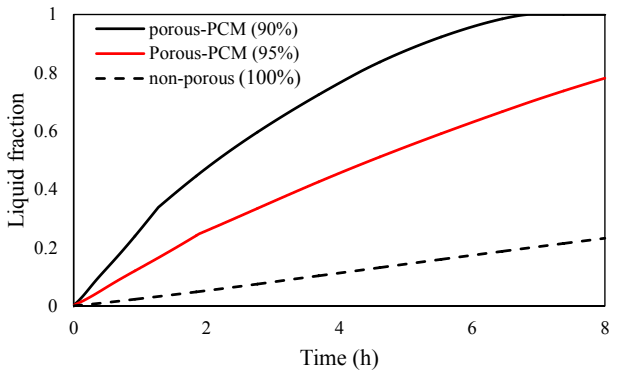

Fig. 8. The time development of the PCM liquid fraction for different porosity of the porous medium.

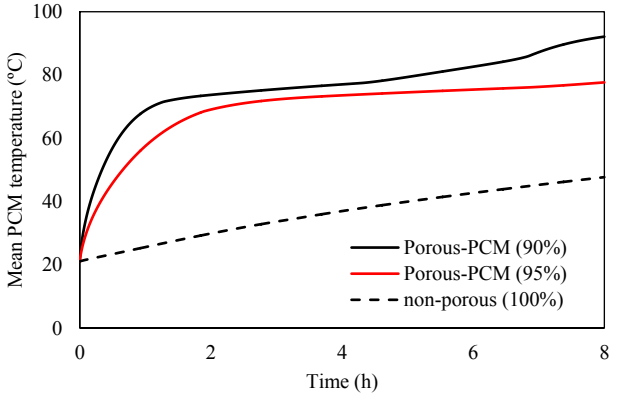

Fig. 9. The time development of the mean PCM temperature for different porosity of the porous medium.

melt the whole PCM. Foam-PCM with lower porosity produces a better melting rate than the case of no porous foam because lower porosity of the metal foam implies a higher ligament volume ratio compared to the pore volume ratio in the overall foam structure. It should be noted that the porosity is selected based on the design parameters. In general, by using a higher porosity material, a higher amount of PCM can be inserted in a constant volume of the storage system. However, the designed system should provide the required output design parameters. Therefore, according to Fig. 8, to store the highest heat capacity in less than 8 h, the metal foam with a porosity of 0.9 should be employed. However, as an example, to reach 78% of the heat capacity in 8 h, the porosity of 95% is enough during the charging mechanism.

The mean PCM temperature profile for the three cases is illustrated in Fig. 9. The mean temperature of PCM increases with time in the case of non-porous-PCM due to absorbing the potential heat. For porous-PCM combinations, there is an early initial surge in the PCM mean temperature that eventually comes to saturate at some point later. It is due to the rate of heat absorption by phase change is low during the early stages as the major part of PCM is still in the solid phase. As soon as the energy distributed in the matrix of the porous foam produces sufficiently and high mean temperature melting becomes widespread, the mean temperature rising little. As shown, the porous case with lower porosity and as a result higher metal shows higher temperature due to the higher rate of heat transfer.

5.2. Discharging mechanism using different air mass flow rates

Fig. 10 compares the transient variation of liquid fraction for three different cases of airflow rate of 0.01, 0.02 and 0.03 kg/s. The solidification rate of PCM is proportional to the flow rate. Increasing airflow causes a larger release of latent heat from the PCM accelerating solidification.

The PCM temperature evolution histories for the three flow-rate values of 0.01, 0.02 and 0.03 kg/s are displayed in Fig. 11. Through the solidification process, there is no significant impact of the variation of airflow rate on the PCM mean temperature during solidification. Temperature decreases most rapidly initially for the flow rate of 0.03 kg/s, followed by the case of 0.02 kg/s, and 0.01 kg/s. For a faster temperature response of PCM, a higher flow rate on the cooling fluid side should be considered. The sharp drop at the time of 8 h is related to the start of the discharging process when the PCM temperature is higher than the melting temperature and thus the PCM places in the sensible heat domain until reaching the phase change domain. For the higher flow rate (0.03 kg/s), the HTF gains more heat from the wall causing the higher drop in the wall temperature and higher temperature difference between the wall and the PCM, consequently, more heat transfers from the PCM to the wall causing the sharper drop in the PCM temperature.

The time histories of the output air temperature for the three flow-rate values of 0.01, 0.02 and 0.03 kg/s are presented in Fig. 12. Increasing the air flow rate significantly reduces the mean output temperature, which is almost at a constant rate. There is an initial decline in the air mean temperature during the early stage of solidification that eventually comes to vanish at some specific point of the solidification time at approximately t = 10.4, 9.6 and 9.1 h for the cases of the flow rate of 0.01, 0.02 and 0.03 kg/s, respectively. Air output temperature is almost constant after these points. The rate of heat recovery from phase change is low during the early duration as most of the PCM remains liquid. When solidification becomes significant, the PCM releases heat to the cooling fluid at constant temperature causing the mean air temperature to proceed without significant change.

Fig. 13 depicts the impact of the air flow on the heat transfer rate inside the TES system, which noticeably increases with increasing the air

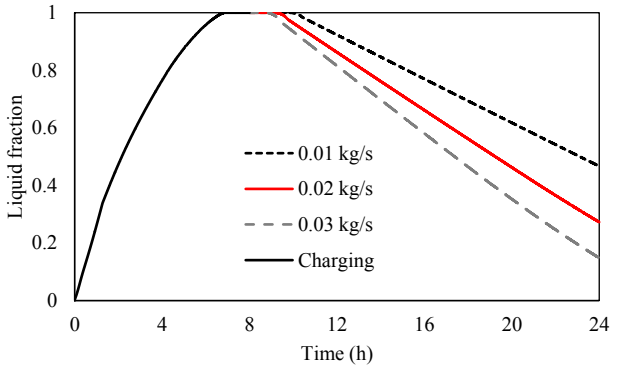

Fig. 10. The development of the PCM liquid fraction through the melting and solidification processes for different air mass flow rates.

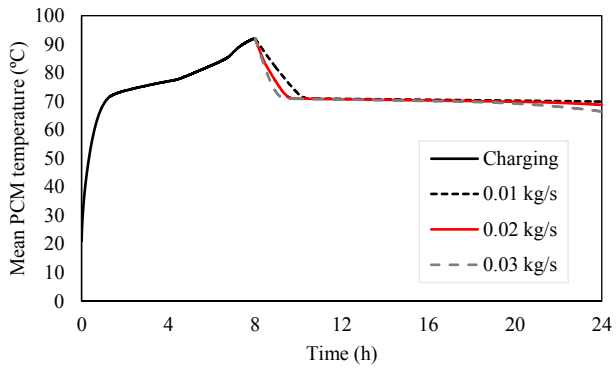

Fig. 11. The development of the mean PCM temperature through the melting and solidification processes for different air mass flow rates.

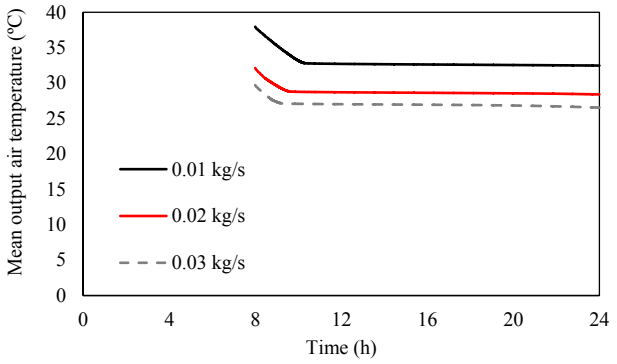

Fig. 12. The development of the mean output air temperature through the solidification process for different air mass flow rates.

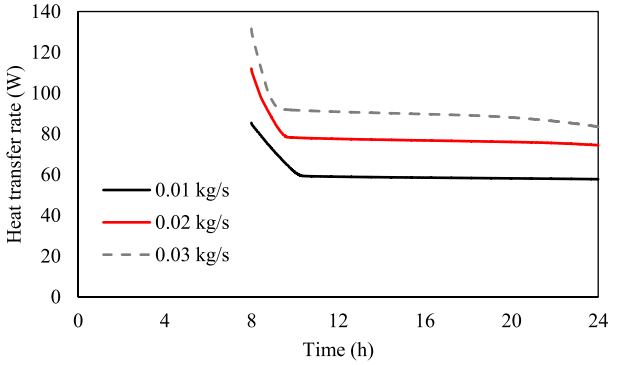

Fig. 13. The development of the heat transfer rate through the solidification process for different air mass flow rates.

flow in the range from 0.01 to 0.03 kg/s. The heat transfer rate is approximately 85, 115 and 130 W at the beginning of heat recovery during PCM solidification for the cases of the flow rate of 0.01, 0.02 and 0.03 kg/s, respectively. Later, the heat transfer rate drops to constant values of 60, 80 and 90 W within almost two hours of solidification starting. The system can transfer heat to the air at a constant rate after only two hours of solidification. Generally, the results from Fig. 13 infer that increasing the flow rate of air in the TES system promotes a faster heat transfer rate within the PCM domain over the whole discharging mode.

Table 2 lists the starting and ending PCM temperature as well as the air for different periods for 8 h of charging and 16 h of discharge. The starting and ending temperatures in Table 2 are related to the temperatures at the time of starting and ending of the simulation. For example, for the charging process, the simulation starts when the PCM temperature is 21 °C and after 8 h when the simulation is stopped, the mean PCM temperature is 92.1 °C. For the discharging with the flow rate of 0.01 kg/s, the mean PCM temperatures changes from 92.1 °C (equal to the ending PCM temperature in the charging process) to 69.9 °C after 16 h. The temperature of the air also varies from 37.96 °C to 22.62 °C during 16 h of discharge. Data from the table show that the reduction in the PCM temperature increases as the flow rate increases during the discharging mode. Furthermore, higher output temperature of the air can be better achieved when the air flow rate is reduced during the discharging mode. For example, after 16 h, the mean PCM temperature difference reduces by 22.2, 23.4, and 25.7 °C for airflow rates of 0.01, 0.02 and 0.03 kg/s, respectively. Furthermore, by increasing the rate of airflow, the outlet air temperature increases by 4.3, 2.7, and 2.0 °C for airflow rates of 0.01, 0.02 and 0.03 kg/s, respectively. This means that there is almost a 24% to 28% rise in the mean PCM temperature due to the increase of the air flow rate from 0.01 to 0.03 kg/s. Meanwhile, there is an increase in the outlet air temperature between 13% and 7% when the airflow rate varies between 0.01 and 0.03 kg/s. Therefore, the potential of the porous-PCM to improve the thermal performance of the air heater is largely affected by the heat transfer and the airflow rates in use during the charging and discharging mode.

5.3. Changing the operation mode

A heating system for space heating usually works for 8 h during the day when people are at spending their time at home. As a storage heater, due to the lower cost of electricity during the night and also the peak-shaving concept, it is preferable to charge the system during the night for 8 h in separate charging/discharging mode. Therefore, 16 h is selected as the total working time of the system in this study. Furthermore, by introducing simultaneous charging/discharging, it is possible to reduce the size of the heater providing similar performance with separate charging/discharging which is more suitable for peak-shaving. This study introduced the concept of simultaneous charging/discharging of the storage heaters to evaluate the behaviour of such a system for domestic space heating. As a result, three different modes of operation are considered in this study to assess how changing mode of operation could affect the thermal efficiency of the HE-PCM unit. These modes are: (I) 8-hour charging and 8-hour discharging separately, (II) 2-hour charging and 2-hour discharging separately for 8 heating cycles, and (III) 2-hour charging and 14-hour discharging simultaneously. In all modes, the mass flow rate and the inlet temperature of the air are set to 0.02 kg/s and 21 °C, respectively. The time histories of the liquid-fraction contours for the HE-PCM system corresponding to the three modes of operation, i.e Mode I, Mode II, and Mode III are presented in Figs. 5-7, Fig. 14, and Fig. 15, respectively. At the early stages ($t \leq 4$ h) of operation, the solid–liquid interface is almost the same in each case. This implies that the propagation speed of melting is still not effective enough to cause a difference in the melting fraction of PCM between the modes in consideration. Typically, heat transfer by conduction mainly dominates this early stage as an effective role of natural convection has not started yet.

As time proceeds to ($t \geq 4$ h), more and more thermal energy moves into the PCM to promote a further dominating role for natural convection over conduction and assists a larger melting fraction during all three modes to start arising. In all modes, the melting fraction persists to be larger compared to earlier stages but different in size between the three modes of operation. A noticeable difference can be detected in the propagation speed of the solid–liquid phase interface by comparing

Table 2
Characteristics of the system using different air flow rates.

Mode	Duration (h)	Heat transfer rate (W)	Starting PCM temperature (°C)	Ending PCM temperature (°C)	Starting Air temperature (°C)	Ending Air temperature (°C)
Charging	8	258.8	21	92.1	–	–
Discharging (0.01 kg/s)	16	−58.9	92.1	69.9	37.96	33.62
Discharging (0.02 kg/s)	16	−75.9	92.1	68.75	32.13	29.48
Discharging (0.03 kg/s)	16	−87.76	92.1	66.43	29.71	27.74

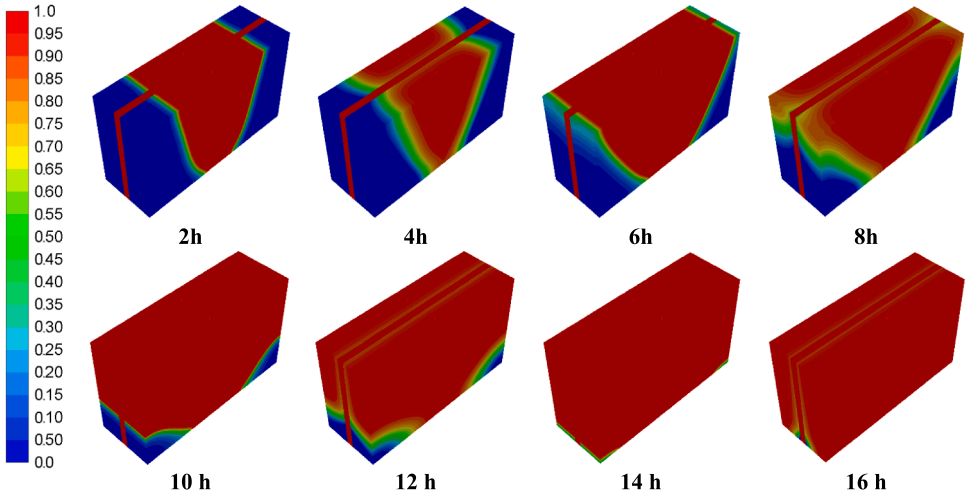

Fig. 14. Liquid-fraction contours for the HE-PCM system corresponding to Mode II (2-hour charging and 2-hour discharging separately for 16 h).

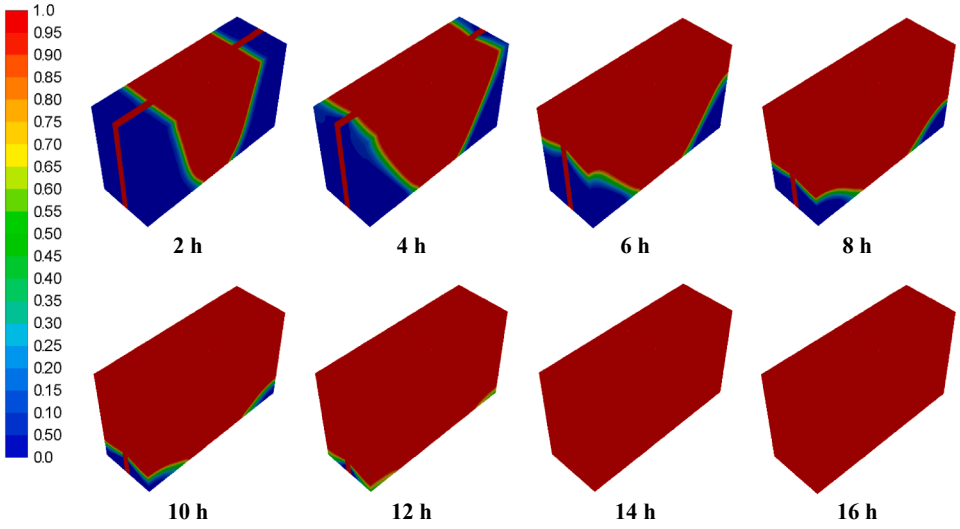

Fig. 15. Liquid-fraction contours for the HE-PCM system corresponding to Mode III (2-hour charging and 14-hour charging/discharging simultaneously).

Mode I and Mode II. Although both undergo a separate charging-discharging approach, the solid–liquid interface of Mode I spreads much faster than that of Mode II. For example, at the time interval of t = 8 h, all PCM is melted for Mode I, while a significant proportion of PCM is still in the solid phase for Mode II. This is attributed to the longer charging period available to mode I compared to mode II in the first 8 h. Meanwhile, a very different trend can be noticed for Mode III compared to the other modes. The charging process is noticeably more dominant than the discharging process during Mode III. This dominating trend of charging over the discharging process lasts over the whole period of operation. In the final stage of operation (t ≥ 14 h), the melted layer of PCM proceeds growing in size to invade the major part of the domain in all modes. However, melting is fully terminated due to the faster charging rate during Mode I and Mode III as compared to that during Mode II. This can be noticed in Fig. 15 (t = 16 h) when the melting speed seems to be a little delayed in the lower part of the domain.

The time-varying liquid-fraction profiles for the three operation modes are shown in Fig. 16. The behaviour curves show a continuous increase in liquid fraction during the charging part within the first 10 h of the operation. Comparing the slope of the curves of the three modes of operation, it can be generally recognized that the melting rate in Mode I is the fastest during this period. The longer charging duration available

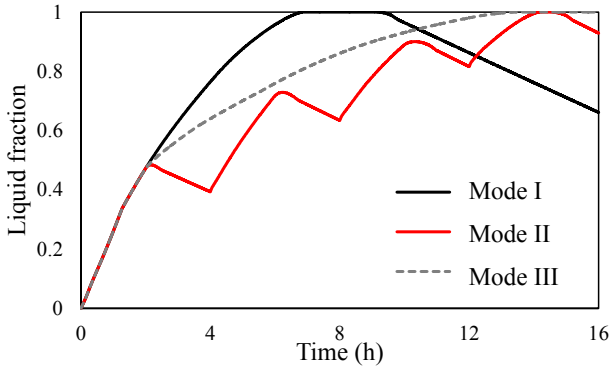

Fig. 16. Timewise variation of liquid fraction for the three modes of operation.

for Mode I supports a faster heat transfer rate from the heating element towards the PCM. Regardless of the mode, the melting occurs at the same rate during the early period operation (t ≤ 3 h), which is because of the nonappearance of free convection during this period of operation. Continuing to the last period of operation (t ≥ 8 h), contrary to the other modes, the curve of Mode I shows a continuous decline of the slope until

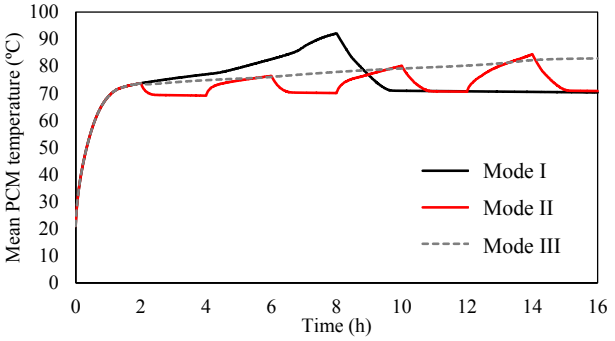

Fig. 17. Timewise variation of average PCM temperature for the three modes of operation.

the end of operation as a sign of the discharging part of the process.

The effects of changing the mode of operation on the mean PCM temperature profile are presented in Fig. 17. Due to the nature of the operation, there is an expected increase in the slope of the temperature curve for Mode I during charging for 8 h, followed by a decline in the slope during discharging. A similar trend but occurring over a shorter time interval is seen in Mode II. In this mode, there is always an increase followed by a decrease in the slope of the temperature curve recurring over every 2-h interval. A very different trend is seen for the simultaneous operation mode (Mode III). In Mode III, the slope of the temperature curve no longer exists as the uniform temperature profile is almost preserved over the whole operation. This stable/constant temperature behavior of the PCM during the simultaneous operation mode is expected to deliver the uniform heat exchange between the PCM and the working fluid (air), as can be detected in Fig. 17.

The timewise variations of the average outlet air temperature related to the different operation modes are shown in Fig. 18. Under the separate charging-discharging operation conditions of Mode I and Mode II, the lines show a slight drop in the average air temperature through the solidification process because of the temperature drop in the PCM as a result of the thermal energy released to the air. Note that the outlet of the air channel is blocked during the charging process in the separate operation of the system (Modes I and II) and therefore the outlet air temperature is not reported during charging. The air temperature drops sharply at the starting of the solidification process when the PCM is in the sensible heat state. During the solidification and phase change process, a negligible drop is detected because of the presence of porous medium and the constant temperature of PCM during the phase change mechanism. Meanwhile, the behavior of the air temperature under the simultaneous charging-discharging operation conditions of Mode III is completely different. The air temperature for both the charging and discharging processes remains stable and uniform as a result of similar PCM behavior. The steady actions of the passage air temperature indicate that the contribution of natural convection to the overall heat exchange between the PCM and the air is very small. This indicates that the dominance of free convection over thermal conduction is no longer effective in the simultaneous mode of operation. Such behavior for the outlet air temperature is very beneficial to the operation of domestic air heaters. It confirms the possibility of obtaining a continuous and stable temperature of the outlet air under the simultaneous charging-discharging operation of PCM-based domestic air-heater applications.

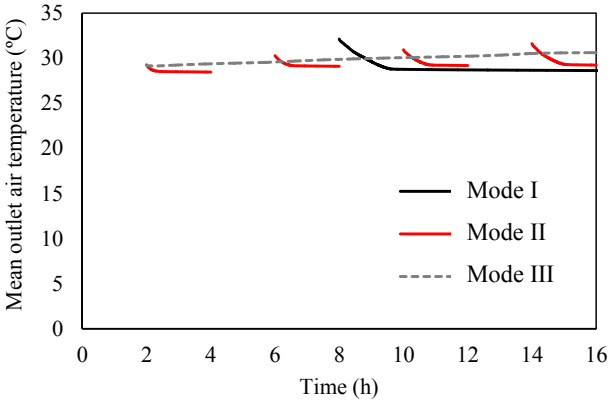

Fig. 18. timewise variation of mean outlet air temperature for the three modes of operation.

6. Conclusion

A two-dimensional numerical investigation of the charging and discharging processes performance in Aluminum metal foam composite and organic phase change material type RT70HC (RUBITHERM) has been investigated. The effects of different operational modes, porous medium, and the air flow rate on the latent-heat storage system were assessed. Results disclosed that the solid–liquid interface of Mode I (charge 8 h, separate discharge 16 h) expands faster than that of Mode II (charge 2 h, discharge 2 h repeated). The charging process is noticeably more dominant than the discharging process during Mode III (charge 2 h, discharge 14 h while still charging). For all the modes, the melting happens significantly during the early period operation ($t \leq 3$ h), due to the presence of the porous medium. Mode III presented the most uniform temperature profile, which caused a uniform heat exchange between the PCM and the air. This stable behaviour of the outlet air temperature implies that the impact of free convection in the wax on the overall heat exchange between the PCM and the air is very small. Decreasing the porosity accelerated the liquid development, after 6.5 h all the PCM became liquid with a mean temperature of 92.1 °C in case of the porosity equals 90%. However, at 95% of porosity, the liquid fraction was 0.78 at the end of the charging period (8 h) with the mean PCM temperature of 78 °C. The PCM temperature reached 92.1 °C after the charging process. With increasing the air flow rates from 0.01 kg/s to 0.03 kg/s, the eventual mean PCM temperature changed from 69.9 °C to 66.43 °C, respectively. This study provided guidelines to minimize the size of the storage heaters by introducing a simultaneous charging/discharging mechanism for domestic space heating applications. The studied parameters could be expanded in future work to enhance the performance of the system including pore density, inlet temperature, nanoparticles addition, even using different PCM layers.

Declaration of Competing Interest

The authors declare that they have no known competing financial interests or personal relationships that could have appeared to influence the work reported in this paper.

References

[1] H. Zhang, M. Sun, L. Song, J. Guo, L. Zhang, Fate of NaClO and membrane foulants during in-situ cleaning of membrane bioreactors: Combined effect on thermodynamic properties of sludge, Biochemical engineering journal 147 (2019) 146–152.
[2] H. Zhang, W. Guan, L. Zhang, X. Guan, S. Wang, Degradation of an Organic Dye by Bisulfite Catalytically Activated with Iron Manganese Oxides: The Role of Superoxide Radicals, ACS Omega 5 (2020) 18007–18012.
[3] F. Yin, X. Xue, C. Zhang, K. Zhang, J. Han, B. Liu, J. Wang, J. Yao, Multifidelity genetic transfer: an efficient framework for production optimization, SPE J (2021) 1–22.
[4] G. Wei, G. Wang, C. Xu, X. Ju, L. Xing, X. Du, Y. Yang, Selection principles and thermophysical properties of high temperature phase change materials for thermal energy storage: A review, Renewable and Sustainable Energy Reviews 81 (2018) 1771–1786.
[5] M. Telkes, Thermal storage for solar heating and cooling, in: Proceedings of the Workshop on Solar Energy Storage Subsystems for the Heating and Cooling of Buildings, Charlottesville (Virginia, USA), 1975.
[6] H. Akeiber, P. Nejat, M.Z.A. Majid, M.A. Wahid, F. Jomehzadeh, I.Z. Famileh, J. K. Calautit, B.R. Hughes, S.A. Zaki, A review on phase change material (PCM) for

sustainable passive cooling in building envelopes, Renewable and Sustainable Energy Reviews 60 (2016) 1470–1497.
[7] Z. Wang, F. Qiu, W. Yang, X. Zhao, Applications of solar water heating system with phase change material, Renewable and Sustainable Energy Reviews 52 (2015) 645–652.
[8] L. Nkhonjera, T. Bello-Ochende, G. John, C.K. King'ondu, A review of thermal energy storage designs, heat storage materials and cooking performance of solar cookers with heat storage, Renewable and Sustainable Energy Reviews, 75 (2017) 157-167.
[9] P.T. Sardari, R. Babaei-Mahani, D. Giddings, S. Yasseri, M.A. Moghimi, H. Bahai, Energy recovery from domestic radiators using a compact composite metal Foam/PCM latent heat storage, Journal of Cleaner Production 257 (2020), 120504.
[10] H. Michels, R. Pitz-Paal, Cascaded latent heat storage for parabolic trough solar power plants, Solar energy 81 (2007) 829–837.
[11] A.S. Mahmood, Experimental Study on Double-Pass Solar Air Heater with and without using Phase Change Material, Journal of Engineering 25 (2019) 1–17.
[12] T. Silva, R. Vicente, F. Rodrigues, Literature review on the use of phase change materials in glazing and shading solutions, Renewable and Sustainable Energy Reviews 53 (2016) 515–535.
[13] E. Oró, A. De Gracia, A. Castell, M. Farid, L. Cabeza, Review on phase change materials (PCMs) for cold thermal energy storage applications, Applied Energy 99 (2012) 513–533.
[14] Z. Zhang, J. Wang, X. Feng, L. Chang, Y. Chen, X. Wang, The solutions to electric vehicle air conditioning systems: A review, Renewable and Sustainable Energy Reviews 91 (2018) 443–463.
[15] A. Arshad, M. Jabbal, P.T. Sardari, M.A. Bashir, H. Faraji, Y. Yan, Transient simulation of finned heat sinks embedded with PCM for electronics cooling, Thermal Science and Engineering Progress (2020), 100520.
[16] J.M. Mahdi, R. Pal Singh, H.M. Taqi Al-Najjar, S. Singh, E.C. Nsofor, Efficient thermal management of the photovoltaic/phase change material system with innovative exterior metal-foam layer, Solar energy 216 (2021) 411–427.
[17] A. Arshad, M. Jabbal, H. Faraji, P. Talebizadehsardari, M.A. Bashir, Y. Yan, Numerical study of nanocomposite phase change material-based heat sink for the passive cooling of electronic components, Heat and Mass Transfer (2021) 1–15.
[18] M. Sun, L. Yan, L. Zhang, L. Song, J. Guo, H. Zhang, New insights into the rapid formation of initial membrane fouling after in-situ cleaning in a membrane bioreactor, Process Biochemistry 78 (2019) 108–113.
[19] N.I. Ibrahim, F.A. Al-Sulaiman, S. Rahman, B.S. Yilbas, A.Z. Sahin, Heat transfer enhancement of phase change materials for thermal energy storage applications: A critical review, Renewable and Sustainable Energy Reviews 74 (2017) 26–50.
[20] X. Liu, R. Rao, J. Shi, J. He, Y. Zhao, J. Liu, H. Du, Effect of oxygen vacancy and A-site-deficiency on the dielectric performance of BNT-BT-BST relaxors, Journal of Alloys and Compounds 159999 (2021).
[21] Y. Liu, Z. Wei, B. Zhong, H. Wang, L. Xia, T. Zhang, X. Duan, D. Jia, Y. Zhou, X. Huang, O-, N-Coordinated single Mn atoms accelerating polysulfides transformation in lithium-sulfur batteries, Energy Storage Materials 35 (2021) 12–18.
[22] R. Bayón, E. Rojas, L. Valenzuela, E. Zarza, J. León, Analysis of the experimental behaviour of a 100 kWth latent heat storage system for direct steam generation in solar thermal power plants, Applied Thermal Engineering 30 (2010) 2643–2651.
[23] L. Yang, H. Peng, X. Ling, H. Dong, Numerical analysis on performance of naphthalene phase change thermal storage system in aluminum plate-fin unit, Heat and Mass Transfer 51 (2015) 195–207.
[24] M.K. Rathod, J. Banerjee, Thermal performance enhancement of shell and tube Latent Heat Storage Unit using longitudinal fins, Applied Thermal Engineering 75 (2015) 1084–1092.
[25] A. Sciacovelli, F. Gagliardi, V. Verda, Maximization of performance of a PCM latent heat storage system with innovative fins, Applied Energy 137 (2015) 707–715.
[26] A.A. Al-Abidi, S. Mat, K. Sopian, M. Sulaiman, A.T. Mohammad, Internal and external fin heat transfer enhancement technique for latent heat thermal energy storage in triplex tube heat exchangers, Applied Thermal Engineering 53 (2013) 147–156.
[27] S. Hosseinizadeh, F. Tan, S. Moosania, Experimental and numerical studies on performance of PCM-based heat sink with different configurations of internal fins, Applied Thermal Engineering 31 (2011) 3827–3838.
[28] X.-Y. Li, L. Yang, X.-L. Wang, X.-Y. Miao, Y. Yao, Q.-Q. Qiang, Investigation on the charging process of a multi-PCM latent heat thermal energy storage unit for use in conventional air-conditioning systems, Energy 150 (2018) 591–600.
[29] A.M. Sefidan, A. Sojoudi, S.C. Saha, M. Cholette, Multi-layer PCM solidification in a finned triplex tube considering natural convection, Applied Thermal Engineering 123 (2017) 901–916.
[30] S. Mehryan, M. Vaezi, M. Sheremet, M. Ghalambaz, Melting heat transfer of power-law non-Newtonian phase change nano-enhanced n-octadecane-mesoporous silica (MPSiO2), International Journal of Heat and Mass Transfer 151 (2020), 119385.
[31] J.M. Mahdi, E.C. Nsofor, Melting of PCM with nanoparticles in a triplex-tube thermal energy storage system, ASHRAE Transactions, 122 (2016) 215+.
[32] C. Zuo, Q. Chen, L. Tian, L. Waller, A. Asundi, Transport of intensity phase retrieval and computational imaging for partially coherent fields: The phase space perspective, Optics and Lasers in Engineering 71 (2015) 20–32.
[33] Z. Hou, H. Lu, Y. Li, L. Yang, Y. Gao, Direct Ink Writing of Materials for Electronics-Related Applications: A Mini Review, Frontiers in Materials 8 (2021) 91.
[34] K. Zhang, Q. Huo, Y.-Y. Zhou, H.-H. Wang, G.-P. Li, Y.-W. Wang, Y.-Y. Wang, Textiles/metal–organic frameworks composites as flexible air filters for efficient particulate matter removal, ACS Applied Materials & Interfaces 11 (2019) 17368–17374.
[35] C. Ho, Y.-C. Liu, M. Ghalambaz, W.-M. Yan, Forced convection heat transfer of Nano-Encapsulated Phase Change Material (NEPCM) suspension in a mini-channel heatsink, International Journal of Heat and Mass Transfer 155 (2020), 119858.
[36] A. Hajjar, S. Mehryan, M. Ghalambaz, Time periodic natural convection heat transfer in a nano-encapsulated phase-change suspension, International Journal of Mechanical Sciences 166 (2020), 105243.
[37] C. Zuo, J. Sun, J. Li, J. Zhang, A. Asundi, Q. Chen, High-resolution transport-of-intensity quantitative phase microscopy with annular illumination, Scientific reports 7 (2017) 1–22.
[38] K. Zhang, J. Zhang, X. Ma, C. Yao, L. Zhang, Y. Yang, J. Wang, J. Yao, H. Zhao, History matching of naturally fractured reservoirs using a deep sparse autoencoder, SPE Journal (2021) 1–22.
[39] J.M. Mahdi, E.C. Nsofor, Melting enhancement in triplex-tube latent heat energy storage system using nanoparticles-metal foam combination, Applied Energy 191 (2017) 22–34.
[40] J.M. Mahdi, H.I. Mohammed, E.T. Hashim, P. Talebizadehsardari, E.C. Nsofor, Solidification enhancement with multiple PCMs, cascaded metal foam and nanoparticles in the shell-and-tube energy storage system, Applied Energy 257 (2020), 113993.
[41] Y. Yang, J. Yao, C. Wang, Y. Gao, Q. Zhang, S. An, W. Song, New pore space characterization method of shale matrix formation by considering organic and inorganic pores, Journal of Natural Gas Science and Engineering 27 (2015) 496–503.
[42] K. Zhang, Z. Yang, X. Mao, X.-L. Chen, H.-H. Li, Y.-Y. Wang, Multifunctional Textiles/Metal− Organic Frameworks Composites for Efficient Ultraviolet Radiation Blocking and Noise Reduction, ACS Applied Materials & Interfaces 12 (2020) 55316–55323.
[43] X. Xue, K. Zhang, K.C. Tan, L. Feng, J. Wang, G. Chen, X. Zhao, L. Zhang, J. Yao, Affine Transformation-Enhanced Multifactorial Optimization for Heterogeneous Problems, IEEE Transactions on, Cybernetics (2020).
[44] B. Zivkovic, I. Fujii, An analysis of isothermal phase change of phase change material within rectangular and cylindrical containers, Solar energy 70 (2001) 51–61.
[45] N. Vyshak, G. Jilani, Numerical analysis of latent heat thermal energy storage system, Energy conversion and management 48 (2007) 2161–2168.
[46] F. Agyenim, N. Hewitt, P. Eames, M. Smyth, A review of materials, heat transfer and phase change problem formulation for latent heat thermal energy storage systems (LHTESS), Renewable and Sustainable Energy Reviews 14 (2010) 615–628.
[47] A. Mosaffa, F. Talati, H.B. Tabrizi, M. Rosen, Analytical modeling of PCM solidification in a shell and tube finned thermal storage for air conditioning systems, Energy and Buildings 49 (2012) 356–361.
[48] Y. Yang, Y. Li, J. Yao, S. Iglauer, L. Luquot, K. Zhang, H. Sun, L. Zhang, W. Song, Z. Wang, Dynamic pore-scale dissolution by CO2-saturated brine in carbonates: Impact of homogeneous versus fractured versus vuggy pore structure, Water Resources Research, 56 (2020) e2019WR026112.
[49] C.-J. Ho, J. Gao, An experimental study on melting heat transfer of paraffin dispersed with Al2O3 nanoparticles in a vertical enclosure, International Journal of Heat and Mass Transfer 62 (2013) 2–8.
[50] Y. Yang, H. Chen, X. Zou, X.-L. Shi, W.-D. Liu, L. Feng, G. Suo, X. Hou, X. Ye, L. Zhang, Flexible carbon-fiber/semimetal Bi nanosheet arrays as separable and recyclable plasmonic photocatalysts and photoelectrocatalysts, ACS Applied Materials & Interfaces 12 (2020) 24845–24854.
[51] V. Kumaresan, R. Velraj, S.K. Das, The effect of carbon nanotubes in enhancing the thermal transport properties of PCM during solidification, Heat and Mass Transfer 48 (2012) 1345–1355.
[52] M. Ghalambaz, A. Doostani, E. Izadpanahi, A.J. Chamkha, Conjugate natural convection flow of Ag–MgO/water hybrid nanofluid in a square cavity, Journal of Thermal Analysis and Calorimetry 139 (2020) 2321–2336.
[53] S. Mehryan, M. Ghalambaz, A.J. Chamkha, M. Izadi, Numerical study on natural convection of Ag–MgO hybrid/water nanofluid inside a porous enclosure: A local thermal non-equilibrium model, Powder Technology (2020).
[54] S. Ebadi, S.H. Tasnim, A.A. Aliabadi, S. Mahmud, Geometry and nanoparticle loading effects on the bio-based nano-PCM filled cylindrical thermal energy storage system, Applied Thermal Engineering 141 (2018) 724–740.
[55] M. Liu, Z. Xue, H. Zhang, Y. Li, Dual-channel membrane capacitive deionization based on asymmetric ion adsorption for continuous water desalination, Electrochemistry Communications 125 (2021), 106974.
[56] R.P. Singh, H. Xu, S. Kaushik, D. Rakshit, A. Romagnoli, Effective utilization of natural convection via novel fin design & influence of enhanced viscosity due to carbon nano-particles in a solar cooling thermal storage system, Solar energy 183 (2019) 105–119.
[57] J.M. Mahdi, E.C. Nsofor, Solidification of a PCM with nanoparticles in triplex-tube thermal energy storage system, Applied Thermal Engineering 108 (2016) 596–604.
[58] J.M. Mahdi, E.C. Nsofor, Multiple-segment metal foam application in the shell-and-tube PCM thermal energy storage system, Journal of Energy Storage 20 (2018) 529–541.
[59] P.T. Sardari, H.I. Mohammed, D. Giddings, M. Gillott, D. Grant, Numerical study of a multiple-segment metal foam-PCM latent heat storage unit: Effect of porosity, pore density and location of heat source, Energy 189 (2019), 116108.
[60] P. Talebizadeh Sardari, H.I. Mohammed, J.M. Mahdi, M. Ghalambaz, M. Gillott, G. S. Walker, D. Grant, D. Giddings, Localized heating element distribution in composite metal foam-phase change material: Fourier's law and creeping flow effects, International Journal of Energy Research (2021).
[61] Y. Yang, L. Tao, H. Yang, S. Iglauer, X. Wang, R. Askari, J. Yao, K. Zhang, L. Zhang, H. Sun, Stress sensitivity of fractured and vuggy carbonate: an X-Ray computed

tomography analysis, Journal of Geophysical Research: Solid Earth, 125 (2020) e2019JB018759.
[62] M. Sun, B. Hou, S. Wang, Q. Zhao, L. Zhang, L. Song, H. Zhang, Effects of NaClO shock on MBR performance under continuous operating conditions, Environmental Science: Water Research & Technology 7 (2021) 396–404.
[63] D. Zhou, C.-Y. Zhao, Y. Tian, Review on thermal energy storage with phase change materials (PCMs) in building applications, Applied Energy 92 (2012) 593–605.
[64] F. Souayfane, F. Fardoun, P.-H. Biwole, Phase change materials (PCM) for cooling applications in buildings: A review, Energy and Buildings 129 (2016) 396–431.
[65] B. Zalba, J.M. Marín, L.F. Cabeza, H. Mehling, Free-cooling of buildings with phase change materials, International journal of refrigeration, 27 (2004) 839-849.
[66] F. Haghighat, Applying energy storage in building of the future, Energy Technology Network (2013) 6–9.
[67] M. Yamaha, S. Misaki, The evaluation of peak shaving by a thermal storage system using phase-change materials in air distribution systems, Hvac&R Research 12 (2006) 861–869.
[68] A. Waqas, S. Kumar, Phase change material (PCM)-based solar air heating system for residential space heating in winter, International journal of green energy 10 (2013) 402–426.
[69] P.T. Sardari, D. Grant, D. Giddings, G.S. Walker, M. Gillott, Composite metal foam/PCM energy store design for dwelling space air heating, Energy conversion and management 201 (2019), 112151.
[70] S. Yao, X. Huang, Study on solidification performance of PCM by longitudinal triangular fins in a triplex-tube thermal energy storage system, Energy 227 (2021), 120527.
[71] Rubitherm GmbH, in, https://www.rubitherm.eu.
[72] S. Esakkimuthu, A.H. Hassabou, C. Palaniappan, M. Spinnler, J. Blumenberg, R. Velraj, Experimental investigation on phase change material based thermal storage system for solar air heating applications, Solar energy 88 (2013) 144–153.
[73] R.T. GmbH, RT70HC data sheet, in.
[74] P. Talebizadeh Sardari, G.S. Walker, M. Gillott, D. Grant, D. Giddings, Numerical modelling of phase change material melting process embedded in porous media: Effect of heat storage size, Proceedings of the Institution of Mechanical Engineers, Part A: Journal of Power and Energy (2019) 1–19.
[75] P. Talebizadeh Sardari, G.S. Walker, M. Gillott, D. Grant, D. Giddings, Numerical modelling of phase change material melting process embedded in porous media: Effect of heat storage size, Proceedings of the Institution of Mechanical Engineers, Part A: Journal of Power and Energy, (2019) 0957650919862974.
[76] ANSYS, ANSYS FLUENT User Guide, 18, in, ANSYS Canonsburg, PA, 2017.
[77] M. Fadl, P.C. Eames, Numerical investigation of the influence of mushy zone parameter Amush on heat transfer characteristics in vertically and horizontally oriented thermal energy storage systems, Applied Thermal Engineering 151 (2019) 90–99.
[78] Z. Liu, Y. Yao, H. Wu, Numerical modeling for solid–liquid phase change phenomena in porous media: Shell-and-tube type latent heat thermal energy storage, Applied Energy 112 (2013) 1222–1232.
[79] Y. Tian, C.Y. Zhao, A numerical investigation of heat transfer in phase change materials (PCMs) embedded in porous metals, Energy 36 (2011) 5539–5546.
[80] C.Y. Zhao, W. Lu, Y. Tian, Heat transfer enhancement for thermal energy storage using metal foams embedded within phase change materials (PCMs), Solar energy 84 (2010) 1402–1412.
[81] A. Abduljalil, S.M. Al-Abidi, Numerical study of PCM solidification in a triplex tube heat exchanger with internal and external fins, Int J Heat Mass Transfer 61 (2013) 684–695.